

SUBJECT AREAS: PHYSICS, MATERIALS SCIENCE, CONDENSED-MATTER PHYSICS, SUPERCONDUCTING PROPERTIES AND MATERIALS

Correspondence and requests for materials should be addressed to *K.K. (kudo@science.okayama-u.ac.jp) or **M.N. (nohara@science.okayama-u.ac.jp)

Superconductivity in $\text{Ca}_{10}(\text{Ir}_4\text{As}_8)(\text{Fe}_2\text{As}_2)_5$ with Square-Planar Coordination of Iridium

Kazutaka Kudo,^{1,*} Daisuke Mitsuoka,¹ Masaya Takasuga,¹ Yuki Sugiyama,² Kento Sugawara,² Naoyuki Katayama,² Hiroshi Sawa,² Hiroaki S. Kubo,¹ Kenta Takamori,¹ Masanori Ichioka,¹ Tatsuo Fujii,³ Takashi Mizokawa,⁴ and Minoru Nohara^{1,**}

¹Department of Physics, Okayama University, Okayama 700-8530, Japan

²Department of Applied Physics, Nagoya University, Nagoya 464-8603, Japan

³Department of Applied Chemistry and Biotechnology, Okayama University, Okayama 700-8530, Japan

⁴Department of Complexity Science and Engineering & Department of Physics, The University of Tokyo, Kashiwa 277-8561, Japan

We report the unprecedented square-planar coordination of iridium in the iron iridium arsenide $\text{Ca}_{10}(\text{Ir}_4\text{As}_8)(\text{Fe}_2\text{As}_2)_5$. This material experiences superconductivity at 16 K. X-ray photoemission spectroscopy and first-principles band calculation suggest Ir(II) oxidation state, which yields electrically conductive Ir_4As_8 layers. Such metallic spacer layers are thought to enhance the interlayer coupling of Fe_2As_2 , in which superconductivity emerges, thus offering a way to control the superconducting transition temperature.

Platinum exhibits a rich variety of coordination geometries. For instance, all of the basic polyhedral forms, including octahedral,¹ triangle-planar,² tetrahedral,³ and square-planar,⁴⁻⁷ can be seen in platinum arsenides.

The diversity of coordination chemistry allows us to synthesize many functional materials, such as superconductors. The following are prominent platinum-arsenide superconductors: SrPt_2As_2 , which consists of PtAs_4 tetrahedra,³ exhibits superconductivity at a transition temperature of $T_c = 5.2$ K,⁸ in which a charge

transfer from donor to acceptor layers⁹ and subsequent emergence of charge-density waves has been discussed;^{3,8} SrPtAs, which consists of PtAs₃ triangles,² shows superconductivity at 2.4 K,¹⁰ for which a broken time-reversal symmetry in a locally noncentrosymmetric structure has been proposed;¹¹ Ca₁₀(Pt₄As₈)(Fe_{2-x}Pt_xAs₂)₅, which consists of PtAs₄ planar squares, exhibits superconductivity at 38 K,⁴⁻⁷ and therefore constitutes a member of the iron-based superconductors.¹²⁻¹⁴ Palladium exhibits similar coordination chemistry;¹⁵⁻¹⁸ Ca₁₀(Pd₃As₈)(Fe_{2-x}Pd_xAs₂)₅ with PdAs₄ planar squares was reported very recently to exhibit superconductivity at 17 K.¹⁸

In contrast, iridium shows limited coordination geometries; only octahedral and tetrahedral coordination are known in arsenides, as in IrAs₃¹⁹ and SrIr₂As₂.³ In this paper, we report the occurrence of square-planar coordination of iridium in a novel iron iridium arsenide Ca₁₀(Ir₄As₈)(Fe₂As₂)₅. This is the first inorganic compound that includes square-planar coordination of iridium. This compound exhibits superconductivity at $T_c = 16$ K. First-principles calculations and X-ray photoelectron spectroscopy (XPS) suggest the presence of iridium (II) oxidation state. The resultant metallic nature of Ir₄As₈ spacer layers will be discussed.

Results

Crystal structure.

Single-crystal structure analysis revealed that the compound, discovered in this study, crystallizes in the tetragonal structure with the space group $P4/n$ (#85) with a chemical composition of Ca₁₀(Ir₄As₈)(Fe₂As₂)₅ (see the Supplementary Tables S1 and S2 for crystallographic data) (CCDC 962099). The atomic ratios of Ca:Fe:Ir:As = 10:10:4:18 are consistent with the results of energy dispersive X-ray spectrometry, 10:9.8:5.8:20.1. The structure consists of alternating stacking of (Fe₂As₂)₅ and Ir₄As₈ layers with five Ca ions between them, as shown in Figure 1. This is isotypic to Ca₁₀(Pt₄As₈)(Fe_{2-x}Pt_xAs₂)₅⁶ or α -(CaFe_{1-x}Pt_xAs)₁₀Pt_{4-y}As₈.⁷ The Fe₂As₂ layers, composed

of edge-sharing FeAs_4 tetrahedra, are the common building block among iron-based superconductors.¹²⁻¹⁴ The Ir_4As_8 layers are unique to the present compound, and act as spacer layers. The size of the Ir square lattice (with an Ir-Ir distance of 4.411 Å) is larger than that of the Fe_2As_2 square lattice (3.860-3.924 Å). This lattice mismatch leads to the formation of the $\sqrt{5} \times \sqrt{5}$ superstructure in the ab -plane, as shown in Figure 1c.

The characteristic square-planar coordination of Ir was found in the Ir_4As_8 layers. There are two Ir sites, as shown in Figure 1b. Ir1 adopts square-planar coordination, resulting in coplanar IrAs_4 squares with a Ir1-As3 bond length of 2.414 Å. On the other hand, Ir2 is at a non-coplanar site with respect to the As_4 square; Ir2 is displaced upward/downward by 0.676 Å toward the As4 ion at the adjacent Fe_2As_2 layer, as shown in Figure 1a. However, the distance between Ir2 and As4 (3.000 Å) is by far longer than the Ir2-As3 bond length (2.441 Å), thus Ir2 can be regarded as adopting square-planar coordination. The corner-sharing Ir1As_3 and Ir2As_3 squares constitute Ir_4As_8 layers, as shown in Figure 1b, where the As3 atoms form As_2 dimers with an As-As bond length of 2.454 Å, which comparable to twice the covalent radius of arsenic that is 2.42 Å.¹⁸ These bond lengths are similar to those in platinum analogue, $\text{Ca}_{10}(\text{Pt}_4\text{As}_8)(\text{Fe}_{2-x}\text{Pt}_x\text{As}_2)_5$:⁷ Corresponding distances, Pt1-As3 = 2.484 Å, Pt2-As4 = 3.087 Å, and Pt2-As3 = 2.415 Å, suggest that the valence state of Ir is similar to that of Pt.

Superconductivity.

Figure 2 shows the temperature dependence of the in-plane electrical resistivity ρ_{ab} of $\text{Ca}_{10}(\text{Ir}_4\text{As}_8)(\text{Fe}_2\text{As}_2)_5$. $\rho_{ab}(T)$ decreases with decreasing temperature, and shows a kink at approximately 100 K. This kink is not due to antiferromagnetic ordering, which is widely observed in iron-based superconductors,¹²⁻¹⁴ since the single-peak structure of the ^{57}Fe -Mössbauer spectrum at 300 K remains unchanged down to 50 K, as shown in the upper inset of Figure 2. At low temperatures, $\rho_{ab}(T)$ exhibits a sharp drop below 20 K, the characteristic of the onset of superconductivity. Zero resistivity was

observed below 17 K. The 10–90% transition width was estimated to be approximately 2 K. The bulk superconductivity was evidenced by the temperature dependence of the magnetization M , shown in Figure 3. $M(T)$ exhibits diamagnetic behavior below 16 K. The shielding signal estimated at 5 K corresponds to 83% of perfect diamagnetism.

Discussion

The observed T_c of 16 K is relatively low among iron-based superconductors.^{12–14} We suggest that $\text{Ca}_{10}(\text{Ir}_4\text{As}_8)(\text{Fe}_2\text{As}_2)_5$ is in an overdoped region. The lower inset of Figure 2 shows the temperature dependence of the Hall coefficient R_H . The negative value suggests that the major carriers are electrons. The small value of R_H as well as the small temperature dependence indicates the overdoping, as inferred from the R_H of $\text{Ba}(\text{Fe}_{1-x}\text{Co}_x)_2\text{As}_2$.²⁰ This is consistent with the absence of antiferromagnetic ordering, which is characteristic of underdoped regions.^{12–14} The consideration of charge neutrality based on the Zintl concept results in the same consequence. Assuming a divalent Ir^{2+} , the present compound is written as $\text{Ca}^{2+}_{10}(\text{Ir}^{2+}_4(\text{As}_2)^{4-}_4)(\text{Fe}^{2+}_2\text{As}^{3-}_2)_5 \cdot 2e^-$; the excess charge $0.2e^-/\text{Fe}$ is intrinsically injected into the superconducting Fe_2As_2 layers. This doping level corresponds to overdoping, judging from the data on doped BaFe_2As_2 .²¹ We expect that a higher T_c can be realized by reducing the intrinsic charge carriers.

Iron-based superconductors reported to date can be characterized by the insulating spacer layers,^{12–14} which include rare-earth oxides²² and alkaline-earth fluorides²³ with a fluorite-type structure, alkali²⁴ or alkali-earth²⁵ ion, and complex metal oxides with combined rock-salt and perovskite-type structures.^{26–30} The insulating spacer layers are stacked in an alternating fashion with superconductive Fe_2As_2 layers, resulting in two-dimensional electronic Fermi surfaces that have been thought to be a key ingredient of high T_c superconductivity.^{12–14} In contrast, the Ir_4As_8 spacer layers of the present compound can be metallic: Figure 4 shows the partial density of states

(pDOS) projections of Fe 3*d* and Ir 5*d* of $\text{Ca}_{10}(\text{Ir}_4\text{As}_8)(\text{Fe}_2\text{As}_2)_5$ from first-principles calculations using the WIEN2k package.³¹ Fe 3*d* predominates in the pDOS at the Fermi energy (E_F), in common with the other iron-based superconductors.³² A remarkable difference is noticeable in the pDOS of the spacer layers; a finite contribution of Ir 5*d* can be seen in the pDOS at E_F , suggesting that the Ir_4As_8 spacer layers are metallic. This is in contrast with the negligible pDOS at E_F of the spacer layers for the other iron-based superconductors,^{12–14,32} including the platinum analogue $\text{Ca}_{10}(\text{Pt}_4\text{As}_8)(\text{Fe}_2\text{As}_2)_5$: The Pt_4As_8 spacer layers are semiconducting because of the opening of the gap in the pDOS of Pt 5*d* at E_F .^{7,33} The difference between the Pt_4As_8 and Ir_4As_8 layers might be attributed to that of the electron configurations; Pt^{2+} ($5d^8$) forms a closed-shell configuration with a completely filled d_{xy} orbital in the square-planar coordination, whereas d_{xy} of Ir^{2+} ($5d^7$) is formally half-filled, resulting in a metallic nature. The oxidation state of iridium (II) is suggested by first-principles calculations, which give an estimate of the total number of electrons of Ir1 and Ir2 (and thus the nominal oxidation states) to be 74.89 ($\text{Ir}^{2.11+}$) and 74.91 ($\text{Ir}^{2.09+}$) from the sum of pDOS up to E_F , respectively. This is consistent with XPS results, as shown in Figure 5: The binding energy at the peak position of Ir 4*f*_{7/2} spectrum suggests that the valence of Ir in $\text{Ca}_{10}(\text{Ir}_4\text{As}_8)(\text{Fe}_2\text{As}_2)_5$ is close to 2+, if we refer to the binding energy of $\text{Ca}_3\text{CoIrO}_6$ ³⁴ with Ir^{4+} and assume that the binding energy is decreased by approximately 1 eV when the valence is decreased by 1 as inferred from the XPS data of K_3IrBr_6 and K_2IrBr_6 .

In cuprates, it has been suggested that the interlayer coupling of superconducting CuO_2 planes enhances T_c .³⁵ The metallic nature of the spacer layers of the present compound $\text{Ca}_{10}(\text{Ir}_4\text{As}_8)(\text{Fe}_2\text{As}_2)_5$ may give rise to an opportunity to engineer the interlayer coupling of superconducting Fe_2As_2 and to thus further enhance the superconducting transition temperature. To do so, we have to develop chemical methods of optimizing the carrier concentration of $\text{Ca}_{10}(\text{Ir}_4\text{As}_8)(\text{Fe}_2\text{As}_2)_5$.

The unusual square-planar coordination of Fe^{2+} has been reported for the oxide SrFeO_2 .³⁶ It has been discussed that strong hybridization or covalent nature between

Fe 3*d* and O 2*p* orbitals for Fe²⁺ in the square-planar coordination is the key ingredient for the stability of SrFeO₂.³⁷ Similar mechanism might be applicable to the formation of the square-planar coordination of Ir²⁺ of Ca₁₀(Ir₄As₈)(Fe₂As₂)₅ because of the strong hybridization between Ir 5*d* and As 4*p* orbitals.

In summary, we found the square-planar coordination of iridium in the Ir₄As₈ layers of the iron iridium arsenide Ca₁₀(Ir₄As₈)(Fe₂As₂)₅. This finding provided a novel iron-based superconductor with $T_c = 16$ K. The optimization of the metallic spacer layer might offer a way to further increase the superconducting transition temperature of iron-based materials.

Methods

Preparation and characterization of samples.

Single crystals of Ca₁₀(Ir₄As₈)(Fe₂As₂)₅ were grown by heating a mixture of Ca, FeAs, IrAs₂, and Ir powders in a ratio of Ca:Fe:Ir:As = 10:10:4:18 or 10:26:14:40. The mixture was placed in an alumina crucible and sealed in an evacuated quartz tube. The manipulation was carried out in a glove box filled with argon gas. The ampules were heated at 700°C for 3 h and then at 1100–1150°C for 10–40 h, after which they were quenched in ice water. The quenching procedure was found to be crucial to obtaining the Ca₁₀(Ir₄As₈)(Fe₂As₂)₅ phase. This process yielded Ca₁₀(Ir₄As₈)(Fe₂As₂)₅ together with a small amount of powder mixture of CaFe₂As₂ and IrAs₂. Plate-like single crystals of Ca₁₀(Ir₄As₈)(Fe₂As₂)₅ with typical dimensions of 0.5 × 0.5 × 0.02 mm³ were separated from the mixture. The crystals were characterized by synchrotron radiation X-ray diffraction,³⁸ energy dispersive X-ray spectrometry, and conventional transmission Mössbauer spectroscopy with a ⁵⁷Co/Rh source.

Electrical resistivity and magnetization measurements.

The electrical resistivity (parallel to the *ab*-plane) and Hall coefficient were measured using the Quantum Design PPMS. Magnetization was measured using the Quantum Design MPMS.

X-ray photoelectron spectroscopy (XPS) measurements.

The single crystals were cleaved under the ultrahigh vacuum for the XPS measurements that were carried out using JEOL JPS9200 analyzer and a Mg K α source (1253.6 eV). The total energy resolution was set to about 1.0 eV. The binding energy was calibrated using the Au 4f core level of the gold reference sample.

1. Thomassen, L. Crystallization of Binary Compounds of Metals of Platinum Group. *Z. Phys. Chem. B* **2**, 349-379 (1929).
2. Wenski, G. & Mewis, A. Trigonal-planar koordiniertes Platin: Darstellung und Struktur von SrPtAs (Sb), BaPtP (As, Sb), SrPt_xP_{2-x}, SrPt_xAs_{0.90} und BaPt_xAs_{0.90}. *Z. Anorg. Allg. Chem.* **535**, 110-122 (1986).
3. Imre, A. et al. Inkommensurabel modulierte Kristallstrukturen und Phasenumwandlungen - Die Verbindungen SrPt₂As₂ und EuPt₂As₂. *Z. Anorg. Allg. Chem.* **633**, 2037-2045 (2007).
4. Kakiya, S. et al. Superconductivity at 38 K in Iron-Based Compound with Platinum-Arsenide Layers Ca₁₀(Pt₄As₈)(Fe_{2-x}Pt_xAs₂)₅. *J. Phys. Soc. Jpn.* **80**, 093704 (2011).
5. Nohara, M. et al. Iron-platinum-arsenide superconductors Ca₁₀(Pt_nAs₈)(Fe_{2-x}Pt_xAs₂)₅. *Solid State Commun.* **152**, 635-639 (2012).
6. Ni, N., Allred, J. M., Chan, B. C. & Cava, R. J. High T_c electron doped Ca₁₀(Pt₃As₈)(Fe₂As₂)₅ and Ca₁₀(Pt₄As₈)(Fe₂As₂)₅ superconductors with skutterudite intermediary layers. *Proc. Natl. Acad. Sci.* **108**, E1019-E1026 (2011).
7. Löhnert, C. et al. Superconductivity up to 35 K in the Iron Platinum Arsenides (CaFe_{1-x}Pt_xAs)₁₀Pt_{4-y}As₈ with Layered Structures. *Angew. Chem. Int. Ed.* **50**, 9195-9199 (2011).
8. Kudo, K., Nishikubo, Y. & Nohara, M. Coexistence of Superconductivity and Charge Density Wave in SrPt₂As₂. *J. Phys. Soc. Jpn.* **79**, 123710 (2010).

9. Zheng, C. & Hoffmann, R. Donor-Acceptor Layer Formation and Lattice Site Preference in the Solid: The CaBe_2Ge_2 Structure. *J. Am. Chem. Soc.* **108**, 3078-3088 (1986).
10. Nishikubo, Y., Kudo, K. & Nohara, M. Superconductivity in the Honeycomb-Lattice Pnictide SrPtAs . *J. Phys. Soc. Jpn.* **80**, 055002 (2011).
11. Goryo, J., Fischer, M. H. & Sigrist, M. Possible pairing symmetries in SrPtAs with a local lack of inversion center. *Phys. Rev. B* **86**, 100507(R) (2012).
12. Ishida, K., Nakai, Y. & Hosono, H. To What Extent Iron-Pnictide New Superconductors Have Been Clarified: A Progress Report. *J. Phys. Soc. Jpn.* **78**, 062001 (2009).
13. Paglione, J. & Greene, R. L. High-temperature superconductivity in iron-based materials. *Nat. Phys.* **6**, 645-658 (2010).
14. Johnston, D. C. The puzzle of high temperature superconductivity in layered iron pnictides and chalcogenides. *Adv. Phys.* **59**, 803-1061 (2010).
15. Brese, N. E. & von Schnering, H. G. Bonding trends in pyrites and a reinvestigation of the structures of PdAs_2 , PdSb_2 , PtSb_2 and PtBi_2 . *Z. Anorg. Allg. Chem.* **620**, 393-404 (1994).
16. Johrendt, D. & Mewis, A. Darstellung und Kristallstrukturen der Verbindungen CaPdAs , CaPdSb und CaPdBi . *Z. Anorg. Allg. Chem.* **618**, 30-34 (1992).
17. Mewis, A. The ThCr_2Si_2 -Type and Related Structures of APd_2X_2 Compounds ($\text{A} = \text{Ca, Sr, Ba}$; $\text{X} = \text{P, As}$). *Z. Naturforsch. B* **39**, 713-720 (1984).
18. Hieke, C. *et al.* Superconductivity and crystal structure of the palladium-iron-arsenides $\text{Ca}_{10}(\text{Fe}_{1-x}\text{Pd}_x\text{As})_{10}\text{Pd}_3\text{As}_8$. *Phil. Mag.* **93**, 3680-3689 (2013).
19. Kjekshus, A. & Pedersen, G. The Crystal Structures of IrAs_3 and IrSb_3 . *Acta. Cryst.* **14**, 1065-1070 (1961).
20. Katayama, N., Kiuchi, Y., Matsushita, Y. & Ohgushi, K. Variation in Electronic State of $\text{Ba}(\text{Fe}_{1-x}\text{Co}_x)_2\text{As}_2$ Alloy as Investigated in Terms of Transport Properties. *J. Phys. Soc. Jpn.* **78**, 123702 (2009).

21. Canfield, P. C., Bud'ko, S. L., Ni, N., Yan, J. Q. & Kracher, A. Decoupling of the superconducting and magnetic/structural phase transitions in electron-doped BaFe₂As₂. *Phys. Rev. B* **80**, 060501(R) (2009).
22. Kamihara, Y., Watanabe, T., Hirano, M. & Hosono, H. Iron-Based Layered Superconductor La[O_{1-x}F_x]FeAs ($x = 0.05$ -0.12) with $T_c = 26$ K. *J. Am. Chem. Soc.* **130**, 3296-3297 (2008).
23. Matsuishi, S. *et al.* Superconductivity Induced by Co-Doping in Quaternary Fluoroarsenide CaFeAsF. *J. Am. Chem. Soc.* **130**, 14428-14429 (2008).
24. Tapp, J. H. *et al.* LiFeAs: An intrinsic FeAs-based superconductor with $T_c = 18$ K. *Phys. Rev. B* **78**, 060505(R) (2008).
25. Rotter, M., Tegel, M. & Johrendt, D. Superconductivity at 38 K in the Iron Arsenide (Ba_{1-x}K_x)Fe₂As₂. *Phys. Rev. Lett.* **101**, 107006 (2008).
26. Zhu, X. *et al.* Sr₃Sc₂Fe₂As₂O₅ as a possible parent compound for FeAs-based superconductors. *Phys. Rev. B* **79**, 024516 (2009).
27. Kawaguchi, N., Ogino, H., Shimizu, Y., Kishio, K. & Shimoyama, J. New Iron Arsenide Oxides (Fe₂As₂)(Sr₄(Sc,Ti)₃O₈), (Fe₂As₂)(Ba₄Sc₃O_{7.5}), and (Fe₂As₂)(Ba₃Sc₂O₅). *Appl. Phys. Express* **3**, 063102 (2010).
28. Zhu, X. *et al.* Transition of stoichiometric Sr₂VO₃FeAs to a superconducting state at 37.2 K. *Phys. Rev. B* **79**, 220512(R) (2009).
29. Ogino, H. *et al.* A new homologous series of iron pnictide oxide superconductors (Fe₂As₂)(Ca_{n+2}(Al, Ti)_nO_y) ($n = 2, 3, 4$). *Supercond. Sci. Technol.* **23**, 115005 (2010).
30. Shirage, P. M. *et al.* Superconductivity at 28.3 and 17.1 K in (Ca₄Al₂O_{6-y})(Fe₂Pn₂) (Pn = As and P). *Appl. Phys. Lett.* **97**, 172506 (2010).
31. Blaha, P., Schwarz, K., Madsen, G. K. H., Kvasnicka, D & Luitz, J. *Wien2k, An Augmented Plane Wave + Local Orbitals Program for Calculating Crystal Properties*, Vienna University of Technology, Wien, (2001).
32. Singh, D. J. & Du, M.-H. Density Functional Study of LaFeAsO_{1-x}F_x: A Low Carrier Density Superconductor Near Itinerant Magnetism. *Phys. Rev. Lett.* **100**, 237003 (2008).

33. Shein, I. R. & Ivanovskii, A. L. *AB INITIO* STUDY OF THE NATURE OF THE CHEMICAL BOND AND ELECTRONIC STRUCTURE OF THE LAYERED PHASE $\text{Ca}_{10}(\text{Pt}_4\text{As}_8)(\text{Fe}_2\text{As}_2)_5$ AS A PARENT SYSTEM IN THE SEARCH FOR NEW SUPERCONDUCTING IRON-CONTAINING MATERIALS. *Theor. Exp. Chem.* **47**, 292-295 (2011).
34. Takubo, K. *et al.* Electronic structure of Ca_3CoXO_6 ($X=\text{Co}, \text{Rh}, \text{Ir}$) studied by x-ray photoemission spectroscopy. *Phys. Rev. B* **71**, 073406 (2005).
35. Sterne, P. A. & Wang, C. S. Higher T_c through metallic inter-layer coupling in $\text{Bi}_2\text{Sr}_2\text{CaCu}_2\text{O}_8$. *J. Phys. C: Solid State Phys.* **21**, L949-L955 (1988).
36. Tsujimoto, Y. *et al.* Infinite-layer iron oxide with a square-planar coordination. *Nature* **450**, 1062-1065 (2007).
37. Tassel, C. & Kageyama, H. Square planar coordinate iron oxides. *Chem. Soc. Rev.* **41**, 2025-2035 (2012).
38. Sugimoto, K. *et al.* Extremely High Resolution Single Crystal Diffractometry for Orbital Resolution using High Energy Synchrotron Radiation at SPring-8. *AIP Conf. Proc.* **1234**, 887-890 (2010).

Acknowledgments

Part of this work was performed at the Advanced Science Research Center, Okayama University. It was partially supported by Grants-in-Aid for Scientific Research (A) (23244074) and (C) (25400372) from the Japan Society for the Promotion of Science (JSPS) and the Funding Program for World-Leading Innovative R&D on Science and Technology (FIRST Program) from the JSPS. The synchrotron radiation experiments performed at BL02B1 and BL02B2 of SPring-8 were supported by the Japan Synchrotron Radiation Research Institute (JASRI; Proposal No. 2012A0083, 2012B0083, 2013A0083, and 2013A1197).

Author contributions

K.K. and M.N. conceived and planned the research. D.M., M.T., and K.K. synthesized single crystals. Y.S., K.S., N.K., and H.S. performed single-crystal structural analysis using synchrotron radiation X-ray diffraction. D.M. and K.K. measured electrical resistivity and magnetization. T.F. carried out Mössbauer spectroscopy. H.S.K., K.T., and M.I. conducted first-principles calculations. T.M. carried out X-ray photoelectron spectroscopy. K.K. and M.N. discussed the results and wrote the manuscript.

Additional information

Supplementary information: Crystallographic data of $\text{Ca}_{10}(\text{Ir}_4\text{As}_8)(\text{Fe}_2\text{As}_2)_5$ is available at <http://www.nature.com/scientificreports>.

Accession Codes: The crystal structure of $\text{Ca}(\text{Ir}_4\text{As}_8)(\text{Fe}_2\text{As}_2)_5$ has been deposited at the Cambridge Crystallographic Data Centre (<http://www.ccdc.cam.ac.uk>). Deposition number is CCDC 962099.

Competing financial interests: The authors declare no competing financial interests.

Figure caption

Figure 1. Crystal structure of $\text{Ca}_{10}(\text{Ir}_4\text{As}_8)(\text{Fe}_2\text{As}_2)_5$ with tetragonal structure [space group $P4/n$ (#85)]. The thick solid lines indicate the unit cell. (a), (b), and (c) show the schematic overviews, Ir_4As_8 layer, and $(\text{Fe}_2\text{As}_2)_5$ layer, respectively. The blue and dark-blue hatches in (b) indicate IrAs_4 squares with coplanar Ir1 and non-coplanar Ir2, respectively. The dashed ellipsoids in (b) represent As_2 dimers.

Figure 2. Temperature dependence of the electrical resistivity ρ_{ab} for $\text{Ca}_{10}(\text{Ir}_4\text{As}_8)(\text{Fe}_2\text{As}_2)_5$. The upper inset shows ^{57}Fe -Mössbauer spectra together with fitted curves. The lower inset shows the temperature dependence of the Hall coefficient R_H .

Figure 3. Temperature dependence of dc magnetization M for $\text{Ca}_{10}(\text{Ir}_4\text{As}_8)(\text{Fe}_2\text{As}_2)_5$ at a magnetic field H of 10 Oe in the zero-field and field cooling conditions.

Figure 4. Electronic density of states (DOS) for $\text{Ca}_{10}(\text{Ir}_4\text{As}_8)(\text{Fe}_2\text{As}_2)_5$. The partial DOS projections (pDOS) of Fe 3d and Ir 5d are shown. The inset shows the pDOS of Ir 5d in the vicinity of the Fermi level E_F .

Figure 5. Ir 4f photoemission spectrum of $\text{Ca}_{10}(\text{Ir}_4\text{As}_8)(\text{Fe}_2\text{As}_2)_5$ taken at 300 K compared to those of $\text{Ca}_3\text{CoIrO}_6$ and IrAs_2 . Broken lines represent the expected peak positions of Ir 4f_{7/2} of Ir^{4+} , Ir^{3+} , and Ir^{2+} for oxides.

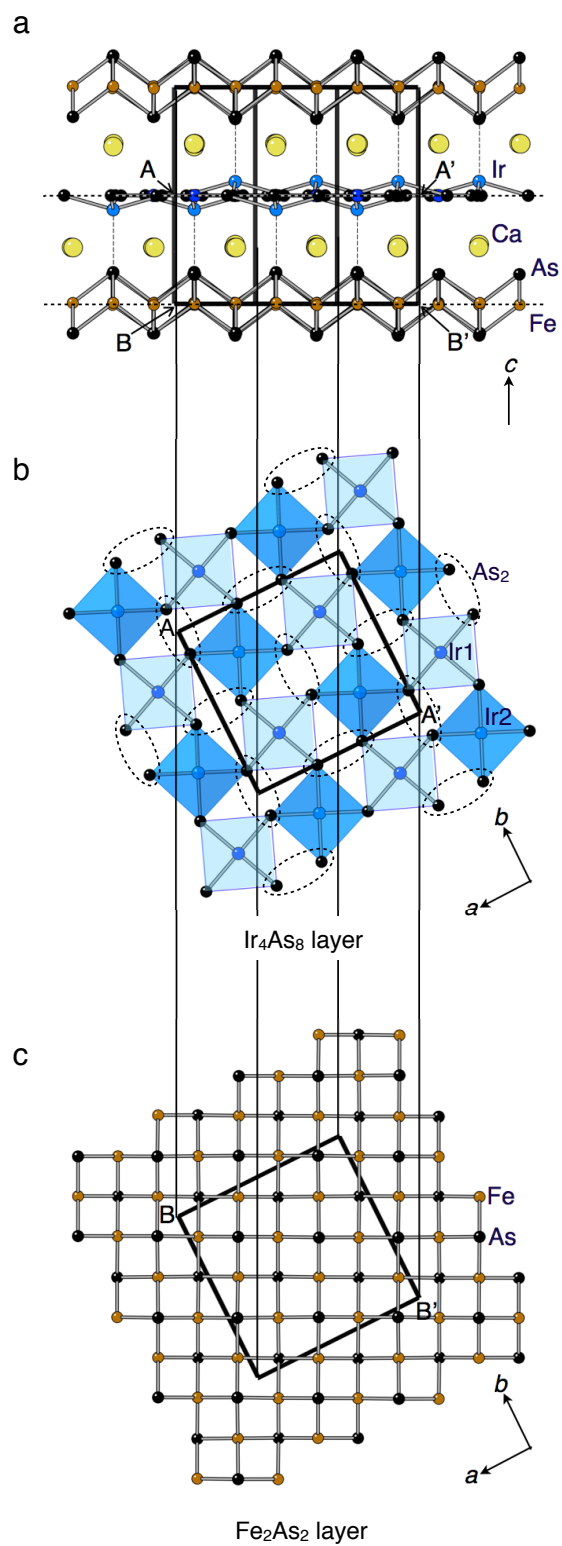


Figure 1

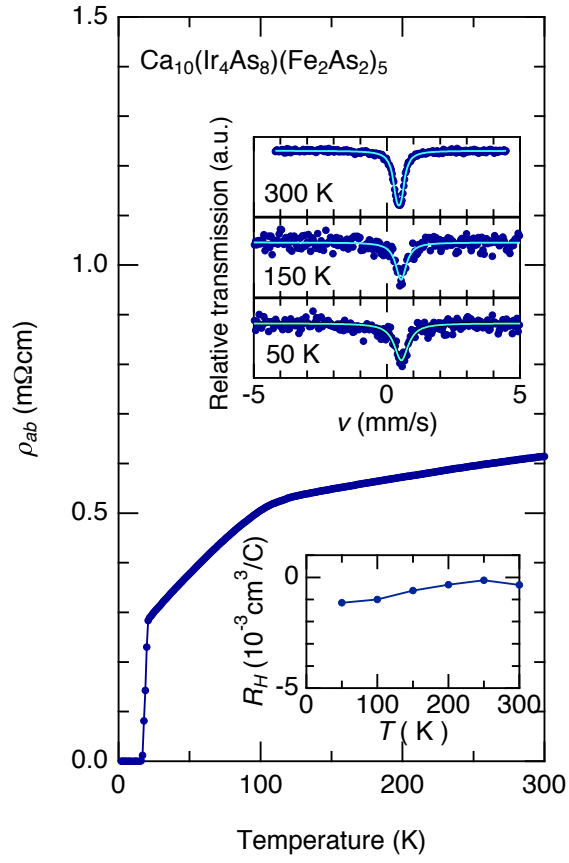


Figure 2

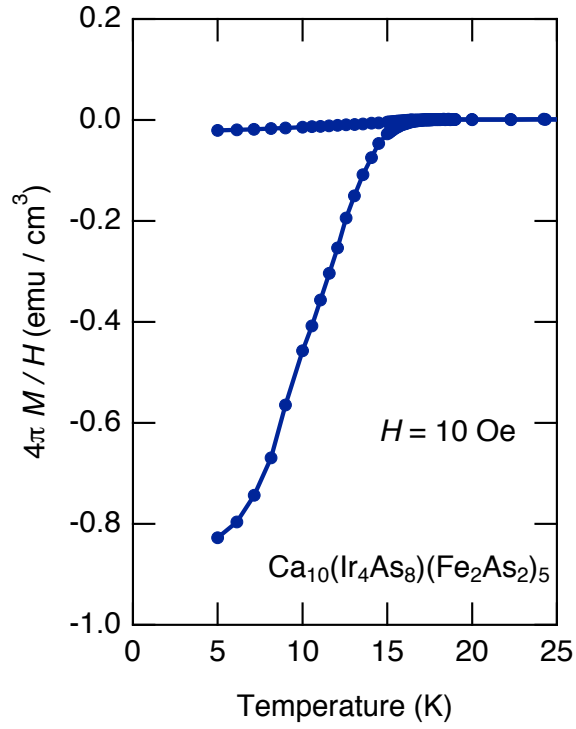


Figure 3

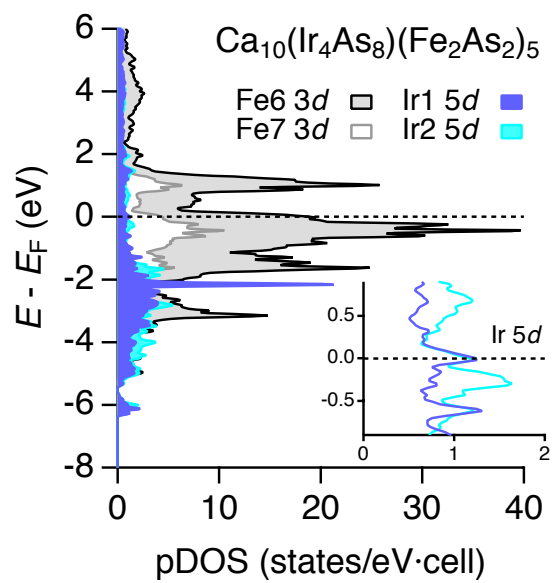


Figure 4

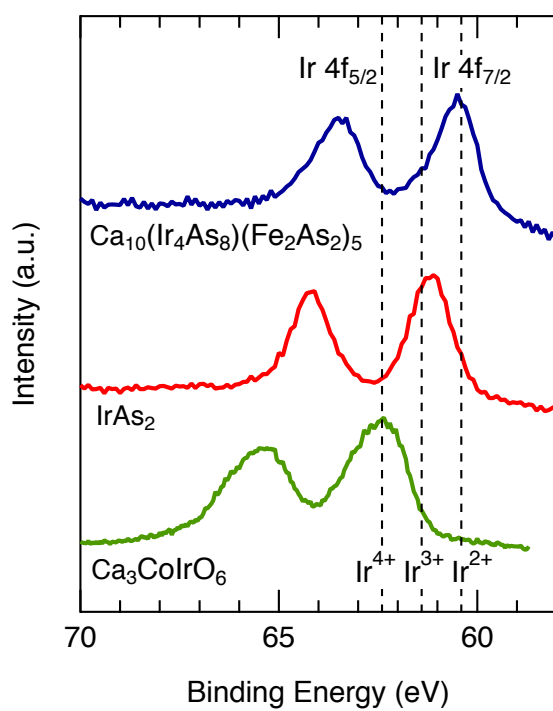


Figure 5

Supplementary Information

Superconductivity in $\text{Ca}_{10}(\text{Ir}_4\text{As}_8)(\text{Fe}_2\text{As}_2)_5$ with Square-Planar Coordination of Iridium

Kazutaka Kudo,¹ Daisuke Mitsuoka,¹ Masaya Takasuga,¹ Yuki Sugiyama,² Kento Sugawara,² Naoyuki Katayama,² Hiroshi Sawa,² Hiroaki S. Kubo,¹ Kenta Takamori,¹ Masanori Ichioka,¹ Tatsuo Fujii,³ Takashi Mizokawa,⁴ and Minoru Nohara¹

¹Department of Physics, Okayama University, Okayama 700-8530, Japan

²Department of Applied Physics, Nagoya University, Nagoya 464-8603, Japan

³Department of Applied Chemistry and Biotechnology, Okayama University, Okayama 700-8530, Japan

⁴Department of Complexity Science and Engineering & Department of Physics, The University of Tokyo, Kashiwa 277-8561, Japan

Table S1. Data collection and refinement statistics for the synchrotron X-ray structure determination of $\text{Ca}_{10}(\text{Ir}_4\text{As}_8)(\text{Fe}_2\text{As}_2)_5$.

$\text{Ca}_{10}(\text{Ir}_4\text{As}_8)(\text{Fe}_2\text{As}_2)_5$	293(2) K
Data Collection	
Crystal System	tetragonal
Space Group	$P4/n$
a (Å)	8.7198(3)
b (Å)	8.7198(3)
c (Å)	10.3768(12)
α, β, γ (°)	90, 90, 90
R_{merge}	0.0772
$I / \sigma I$	> 2
Completeness (%)	0.982
Redundancy	14.2
Refinement	
Resolution (Å)	0.49
No. of Reflections	3476
$R1$	0.0658
No. of Atoms	9

Table S2. Crystallographic parameters of $\text{Ca}_{10}(\text{Ir}_4\text{As}_8)(\text{Fe}_2\text{As}_2)_5$ with the space group $P4/n$ at 293(2) K. The atomic coordinates and thermal parameters were refined. A crystal information file (CIF) of the crystal structure of $\text{Ca}_{10}(\text{Ir}_4\text{As}_8)(\text{Fe}_2\text{As}_2)_5$ derived by the analysis can be obtained free of charge from the Cambridge Crystallographic Data Centre at www.ccdc.cam.ac.uk. CCDC 962099 contains the crystallographic data for this paper.

$\text{Ca}_{10}(\text{Ir}_4\text{As}_8)(\text{Fe}_2\text{As}_2)_5$				
Atomic Positions				
Site	Occupancy	x / a	y / b	z / c
Ir1	1	1/4	3/4	1/2
Ir2	1	3/4	3/4	0.56468(5)
As3	1	0.50426(7)	0.64062(7)	0.49949(5)
As4	1	1/4	1/4	0.14623(12)
As5	1	0.65104(6)	0.45377(6)	0.13589(6)
Fe6	1	0.44779(8)	0.34930(9)	0.00487(6)
Fe7	1	1/4	3/4	0
Ca8	1	0.34543(13)	0.55125(12)	0.26048(12)
Ca9	1	3/4	3/4	0.2733(2)